3-Dimensional Documentation and Visualisation of Resection Specimen and Histopathology in Oral Maxillofacial Oncologic Surgery

JORDAN VERBURG* 1,a | JEROEN VAN RIJSSEL 2,b| dr. ROY VAN DEN ENDE 3,c | dr. ERIC DIK 2,d

1 Technical University Delft, Mekelweg 5, Delft, 2628 CD, The Netherlands.
2 Radboud University Medical Centre, Geert Grooteplein Zuid 10, Nijmegen, 6525 GA, The Netherlands.
3 Leiden University Medical Centre, Albinusdreef 2, Leiden, 2333 ZA, The Netherlands.

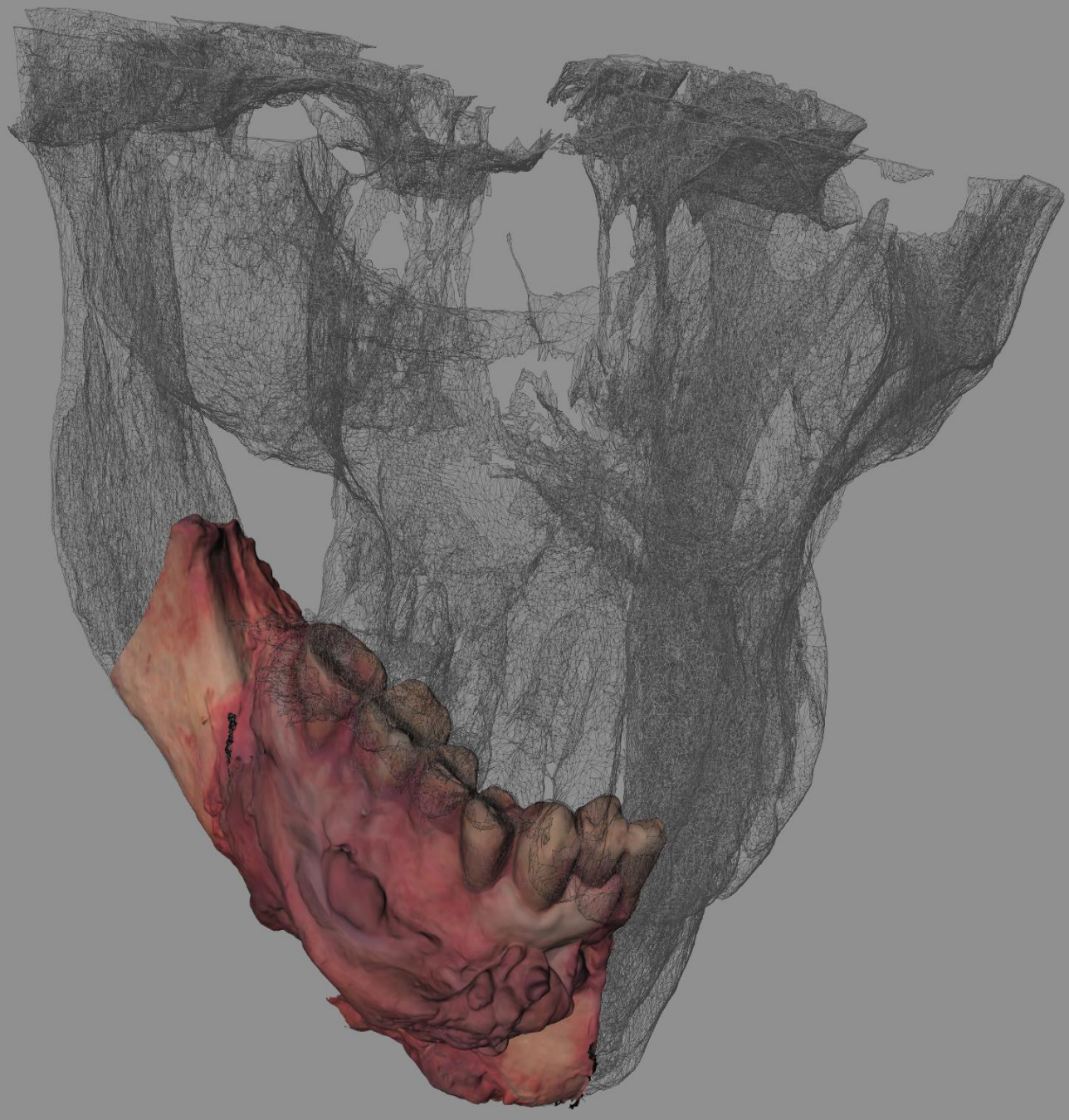

a 3rd year Master student Technical Medicine

b Daily supervisor - Oral and Maxillofacial Fellow

c Medical Supervisor - Oral and Maxillofacial Surgeon

d Technical Supervisor - Technical Physician

Page left intentionally blank.

3-DIMENSIONAL DOCUMENTATION AND VISUALISATION OF RESECTION SPECIMEN AND HISTOPATHOLOGY IN ORAL MAXILLOFACIAL ONCOLOGIC SURGERY

by

Jordan Verburg

Student number : 5419182

2 June 2024

Thesis in partial fulfilment of the requirements for the joint degree of Master of Science in

Technical Medicine

Leiden University ; Delft University of Technology ; Erasmus University Rotterdam

Master thesis project (TM30004 ; 35 ECTS) Dept. of Biomechanical Engineering, TUDELFT

29 January 2024 – 11 June 2024

Feasibility study (15 ECTS):

30 October 2024 – 26 January 2024

Supervisors:	Jeroen van Rijssel (Daily supervisor)	Department of oral maxillofacial surgery, Radboud University Medical Centre, Nijmegen
	Dr. Roy van den Ende (technical supervisor)	3D Lab oral maxillofacial surgery, Leiden University Medical Centre, Leiden
	Dr. Eric Dik (medical supervisor)	Department of oral maxillofacial surgery, Radboud University Medical Centre, Nijmegen
Thesis committee members:	Dr. Brend Jonker (Chair)	Department of oral maxillofacial surgery, ErasmusMC, Rotterdam
	Dr. Roy van den Ende (Technical supervisor)	3D Lab oral maxillofacial surgery, Leiden University Medical Centre, Leiden
	Dr. Eric Dik (Medical supervisor)	Department of oral maxillofacial surgery, Radboud University Medical Centre, Nijmegen

Acknowledgements

I would like to express my sincere gratitude to dr. Miachael Topf[1], for his insights and time. I wish to extend my appreciation to the staff and facilities of the Radboud UMC anatomy department[2], whose resources and assistance were crucial in the completion of this research. Their cooperation and provision of necessary materials significantly contributed to the success of this work.

I am grateful to Markus Wending for his insight into radiotherapy planning, which helped give me the required knowledge to implement findings in that setting.

I thank Professor Hans Kaanders for his enthusiasm and support regarding the potential of this research in the radio-therapeutical setting. Special thanks to Lieke van der Woude and Ilse de Laak-de Vries from the pathology department for allowing me access to the pathology lab and for their time and patience during the 3D scans I performed there.

I also appreciate the help of Thomas Maal, Arico Verhulst, and all the 3D lab colleagues for their openness to questions and collaborative spirit.

Lastly, I am deeply thankful to my supervisors, Jeroen van Rijssel, Eric Dik, and Roy van den Ende, for their guidance, feedback, and support throughout this project.

1

Dr. *Michael Topf MD*
Stanford Medicine | Stanford · Department of Otolaryngology
Doctor of Medicine

2

Dissection rooms
D.E. Doomernik, MD (Head dissection rooms) Department of Medical Imaging, Anatomy
Radboud University Medical Center
Postbus 9101, 6500 HB Nijmegen, The Netherlands (route 102)
www.radboudumc.nl

Table of Content

1

General Introduction

Purpose of this research

This master thesis builds upon previous research conducted at the Radboud UMC for the 3D lab and Oral and maxillofacial surgery (OMFS) department, titled “Exploring a Novel Use of an Intra-Oral Scanner: Improving Methods of Documenting Resection Specimen Orientation in Oral and Maxillofacial Tumour Surgery." The research concluded with the development of a promising preliminary prototype, integrating3-dimensional (3D) scans of surgical resection specimen into CT images, in the surgical resection specimen report.

The purpose of this research was to expand upon the feasibility study, which successfully demonstrated the potential integration of the proposed methodologies and technologies. Firstly, by determining the suitability of various scanners to scan human tissue, integrate histopathological findings and use the resultant models for adjuvant radiotherapy planning. During the second-year internship of the preceding research, an intra oral scanner was used to create the 3D scans. Given the scope of the internship, this choice of scanner was considered reasonable at the time, due to its immediate availability. However, to make a more informed decision regarding the scanner used, several scanners were formally tested (in part driven by the prior literary research), resulting in the purchase and use of the EinScan SP V2 3Dscanner.

Subsequent to this, a new workflow was developed to create 3D models with the new scanner, better suited to both the scanner and the adjusted goals of histopathological incorporation and use on the radiotherapy department. Seeking cooperation with the pathology lab and incorporating their findings of the research specimens into the 3D model,

with the ultimate goal of using the final 3D model within the radiotherapy department to assist with adjuvant radiotherapy planning.

Oral Maxillofacial Oncologic Surgery

Oral and maxillofacial surgery (OMFS) is a distinct domain within surgical practice, which focusses on the diagnosis, surgical intervention, and management of benign and malign tumours of the oral cavity jaw and associated facial structures. Both an understanding of oncologic principles and the complex functional anatomy of the oral maxillofacial region are of importance. Surgical interventions involve the resection of tumours, reconstruction of the affected areas and restoration of function. Careful preoperative planning is required for a successful outcome.

In OMFS, the aim is to ensure histologically clear margins, devoid of tumour cells. Achieving a distance of 5 mm or more between the resection margin and the tumour defines a clear margin, which is vital for minimizing the likelihood of locoregional recurrence. Reconstructive techniques include microvascular free tissue transfers and bone grafting to restore function and aesthetics of areas that have been destructed by tumours or required excision. Furthermore, OMFS requires close collaboration with the radiotherapy team for possible pre- and post-operative radiation therapy, pathologists to interpret surgical resection specimen and radiologists and, in the case of the RadboudUMC, the 3D lab, for accurate preoperative planning.

Surgical Resection Specimen Report

The surgical pathology specimen report, prepared by the surgeon after a tumour resection, is sent alongside the specimen to the pathologist for detailed analysis. It includes the anatomical location of the excised tissue by pinning the specimen onto a schematic drawing of the local anatomy, thus relating the specimen's approximate relation to it. Orientation markers or sutures indicate specific margins and anatomical landmarks. The condition of the resection margins is documented, specifying whether they appear clear of tumour.

This report ensures the pathologist has information about the excised tissue and clinical context, aiding in accurate diagnosis and sectioning of the specimen.

The role of 3D scanning

Surface 3D scanners capture three-dimensional images of objects of interest. Used on excised human tissues they can offer a detailed representation of the specimen's anatomy. Integrating 3D scanning could, therefore, improve the understanding of the anatomy of resected specimen, and when combined with CT imaging, the surrounding anatomy.

An important advantage of digital 3D models is that they facilitate more precise measurements and permit multi-angle examination compared to traditional methods, such as regular photography. The digitisation also ensures that data of the resection specimen remains available, even after the destructive process of pathological gross sectioning, whereby the resection specimen is cut into slices for pathological examination.

Moreover, the digital documentation, especially as a 3D model including CT data, could be of value in multidisciplinary discussions, communication between surgical teams and pathologists, and (adjuvant) radiotherapy planning.

2

Clinical Background

Tumours of the mouth

Introduction

Tumours of the mouth encompass a variety of benign and malignant growths originating from the various tissues within the oral cavity. Malignant growths of the oral cavity rank 16th of 33 listed as of 2022 with ~390000 new diagnosed cases as reported by GLOBOCAN (1), compared to a reported incidence of ~270000 cases 20 years prior, in 2002 (2). The most common type of oral malignant tumours are squamous cell carcinomas (SCC), accounting for approximately 90% of all oral cancers (3). Human papillomavirus (HPV) tobacco smoking and alcohol consumption are the most important risk factors, betel quid, a type of chewing narcotic, is an important risk factor in South East Asia and the Indian subcontinent (4) (5), where it is also the most commonly diagnosed cancer, as shown in Figure 1.

Epidemiology

The incidence of oral SCC is more than twice as high in men than in woman globally(6), and typically occurs over the age of 40. (7)

Oral SCC diagnosis epidemiology varies globally, with Asia being heavily overrepresented, having the highest incidence and mortality. Over 65% of new cases and over 70% of all oral SCC related deaths are from Asia. An interesting development in Europe, is that a rise in HPV infections is causing a rise if oral SCC in younger people (7).

Pathology

90% of all malignant oral cancers are squamous cell carcinomas, the remaining 10% consist of malignancies arising from salivary glands, epithelium connective or lymphoid tissue, or in rarer cases, distant metastases. (7).

Premalignant presentations of SCC can be divided into two major groups, leukoplakia and erytrhoplakia. The WHO defines these leukoplakia as “a white patch or plaque that cannot be characterized clinically or pathologically as any other disease” either with or without presence of dysplasia, and erythroplakia similarly as “a bright red velvety patch that cannot be characterized clinically or pathologically as being caused by any other condition”, again either with or without presence of dysplasia (8). In one study (9) dysplasia or malignancy was found to be present in 19.9% of cases of leukoplakia. Erythroplakia, while being less common than leukoplakia, has far higher rates, with a study conducted by the same researchers finding that in 91% of cases the tissue showed either malignancy or dysplasia (10). In other words, when confronted with a patient with signs of a red velvety patch in the oral cavity, with no other underlying cause, is concerning, especially if there is a history of smoking or alcohol consumption.

Histopathological evaluation of tissue biopsies is the gold standard to diagnose and stratify (potential) oral SCC.

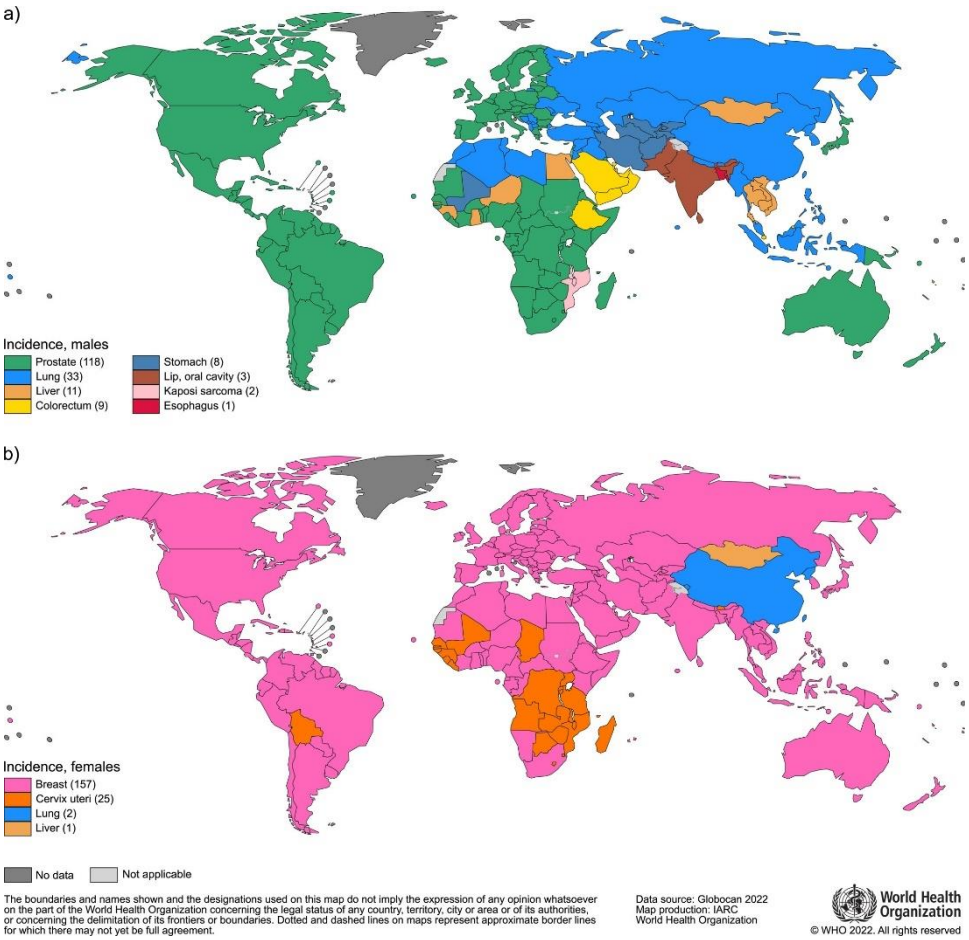

Figure 1: Global map of cancer incidence for male (top) and female (bottom) populations in 2022. Of note is oral cancer being the most incident cancer in the Indian subcontinent. ***Source****: From Bray F, Laversanne M, Sung H, Ferlay J, Siegel RL, Soerjomataram I, et al. Global cancer statistics 2022: GLOBOCAN estimates of incidence and mortality worldwide for 36 cancers in 185 countries. CA Cancer J Clin. 2024;74(3):229-63, used under Creative Commons CC BY-NC-ND license*

Treatment

An in-depth description of the involved and complex methods involved in surgical (and non-surgical) approaches to head and neck oncology is however, beyond the scope of this Master Thesis. Nonetheless, it is useful to have a broad overview of the possibilities and their rationale.

The preferred primary treatment of oral SCCs is surgical resection. The tumour can be removed and then provide information on margin status, spread, histopathology is more detailed than a biopsy and with this extra information helps with the decision making of

subsequent treatment option, such as adjuvant radiotherapy. This is of course reliant on the resectibility of the tumour and requires further considerations of comorbidities that may preclude surgery and patient age and expectations. (2)

Surgical

The surgical approach is curative in intent. Access for small and superficial lesions can be gained transorally. For more invasive tumours of the tongue a paramedian mandibulotomy may need to be performed. Tumours with mandibular or maxillary invasion generally require a more involved approach and are performed via flaps of the upper or lower cheek or visor flaps to gain the access needed to operate. For patients with nodal metastasis in the neck a neck dissection may need to be indicated. (7)

The goal of the surgery is the reconstruction of the oral cavity anatomy. Regular surgical closure will suffice for smaller lesions. For the more complex cases however, free flaps are generally required to reconstruct the affected area. An example and commonly used method of such reconstruction is the fibula free flap procedure for tumours requiring a mandibulectomy.

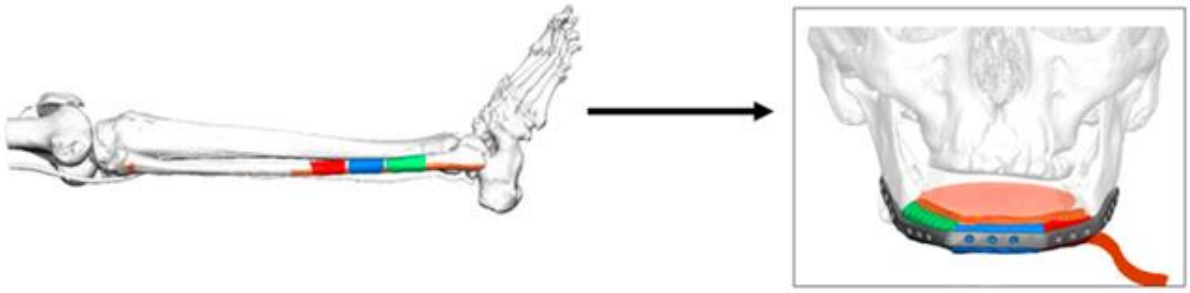

Figure 2: Schematic of a fibula free flap procedure. The fibula bone is partially removed and then cut into parts as required for the reconstruction and guided by a preoperative plan. The sections of fibula are then fixed in place in the mandibula using metal plates and screws. Vascularisation is not shown here but is maintained from the fibula vasculation and used to vascularize the section via microvascular surgery once placed in the mandible. ***Source****: From Knitschke M, Sonnabend S, Backer C, Schmermund D, Bottger S, Howaldt HP, et al. Partial and Total Flap Failure after Fibula Free Flap in Head and Neck Reconstructive Surgery: Retrospective Analysis of 180 Flaps over 19 Years. Cancers (Basel). 2021;13(4), used under Creative Commons CC-BY license.*

Non-surgical

Non-surgical options could include definitive radiotherapy, chemotherapy. A study published in 2020 indicated that intensity-modulated radiation therapy (IMRT) could be a possible curative option for patients who cannot undergo surgery due to, for instance, personal wishes or comorbidities that disallow surgery. (11)

However, a systematic literature review conducted in 2020 investigating non-surgical approaches to oral SCC treatments in light of resource management during the COVID pandemic, determined that primary radiotherapy and primary chemotherapy are inferior to definitive surgical resection. (12)

In the future immunotherapy may prove impactful in primary treatment of oral SCC. Research into this approach is promising, but still in its relative infancy, requiring more investigation before the rational for its use can be supported as evidence based medicine. (13)

Adjuvant radiotherapy

For locoregional control adjuvant radiotherapy may be indicated. This is the case for patients with close or irradical margins, perineural invasion and nodal invasive disease. The goal is to remove any remaining microscopic malignancy that cannot be feasibly surgically removed.

Prognosis

A 2014-2020 report from the US National Cancer Surveillance Epidemiology and End Results program reports a relative 5 year survival rate of 69% (14). This 5-year overall survival rate of surgically treated oral SCC (with and without adjuvant radiotherapy) while having increased over the years, has remained relatively stable for the past decade. An international retrospective study showed an increase of over 10% (from 59 to 70%) over the course of 21 years (1990-2011) (15). The survival rate is dependent on comorbidity, and at time of diagnosis; age of the patient, site of the tumour, stage of the cancer and grade of the oral SCC (16).

Recurrence remains a challenge, with literature reporting a recurrence rate of 28% within a mean time of 24 months after treatment. (17) (18). Local regional recurrence is the most commonly seen type of recurrence, requiring vigilant and timely follow up to be detected (18). It also highlights the importance of margin control during and after tumour removal.

Tumours this research addressed

Oral and maxillofacial oncologic surgery is a complex expertise with many presentations. While 90% of the tumours are squamous cell carcinomas in origin, the varied locations within the oral cavity makes each case unique. For the purpose of this research into creating 3D models registered onto CT data, with inclusion of histopathologic data, the decision was made to focus on tumours with invasion into bony structures requiring surgery, e.g. tumours with mandibular invasion. This decision was made to give the best ability to register the resultant 3D models onto available CT data. This is something that could not be guaranteed in the case of exclusively soft tissue tumours, such as, for example, a SCC of the tongue. As the

focus of this research was first and foremost on the feasibility of creating *any type* of comprehensive 3D model including histopathological data, the choice was made to focus on those cases, which arguably had the best a priori chance for successfully creating such a model.

3

Scanner Comparison

Introduction

Despite a broad array of commercially available 3D scanners, establishing a universal standard for their use in medical contexts remains challenging. In part this is due to the varied nature of medical specimens and the specific requirements of different scanning applications. Consequently, rather than seeking a universally optimal scanner, it was deemed more practical to evaluate the performance of different scanners within specific use cases. This approach allows for an understanding of the strengths and limitations inherent in each scanner design, allowing the most suitable option for any specific use case to be selected.

A literature review performed before this Master Thesis, focussed primarily on 3D scans specific to resection specimens, margin control and head and neck oncologic surgery, showed that there are several approaches to creating 3D scans of human tissue. They range from using micro-computed tomography (micro-CT) (19, 20) and augmented reality (AR) (21) to the use of various forms of surface light scanning or photography (22-33). The most used device was found to be the EinScan SP 3D scanner (Figure 3Figure 3: The EinScan SP V2 by Shinning 3D, shown here during calibration. On the right is the camera used to create the 3D scan, currently attached to a turntable at a fixed distance. On the left the turntable with on it the calibration board used during the calibration process. The camera is attached to the laptop via USB-C for software processing purposes, such as calibration and (post)-processing of recorded 3D models.) (27-30, 32-34). Especially for resection specimen scanning it was reported to be successful. Reasons cited for the choice of this scanner, were its ease of use and affordability. Details regarding specifics of the technical abilities of the scanners were however, generally not considered beyond its ability to create 3D models.

While ease of use is important, and the demonstration of successful use of the EinScan SP to scan resection specimens is promising, this research aimed to formally compare several scanners to come to a more informed decision, based on evidence. As exhaustive research of every commercially available 3D scanner is not feasible, nor within the scope of this project, a decision was made to compare several scanners available from the 3D Lab of the Radboud UMC. The scanners were the EinScan SP, the Einscan H2 and the Einstar 3D, by 3D shining and the TRIOS 3 intraoral scanner (iOS) by 3Shape (35-38). The scanners are intended for use at different scales, with the iOS being intended for the small scale of dentition and the H2 designed for larger structures such as whole-body scanning. The EinScan SP uses a static camera and scans objects placed on a turntable which rotates automatically. The H2, Einstar and iOS require the user to manually move the camera around the object. The technical details of each of the scanners were reported in the feasibility study and can be found in Appendix A of this report.

For this comparison the accuracy and trueness of these four scanners was assessed by scanning specimens taking from a human cadaver and comparing the resultant models from each scanner with each other and to a reference CT scan. Additionally, the scan duration and useability were documented.

Furthermore, several 3D prints were created, and these too were then scanned by each of the four scanners and compared to the dimensions of the 3D prints as measured with digital vernier callipers. This allowed for insight not only into the scanners' ability to scan human resection specimens specifically, but also their ability to scan in general, in absence of confounding factors such as the reflectiveness and colour of human tissue.

Figure 3: The EinScan SP V2 by Shinning 3D, shown here during calibration. On the right is the camera used to create the 3D scan, currently attached to a turntable at a fixed distance. On the left the turntable with on it the calibration board used during the calibration process. The camera is attached to the laptop via USB-C for software processing purposes, such as calibration and (post)-processing of recorded 3D models.

Method

Five specimens were resected from a fresh frozen cadaveric head obtained from the Radboud UMC anatomy department (39) by an experienced Fellow oral maxillofacial surgeon. The resections made consisted of wo mandibular resections (one hemimandibulectomy and one partial mandibulectomy), two maxillary resections (one including the orbita floor, one without) and one tongue resection. The choice for these specimens was based on selecting specimens as they would typically be seen in the Radboud UMC surgical setting. Figure 4 shows the specimens after resection.

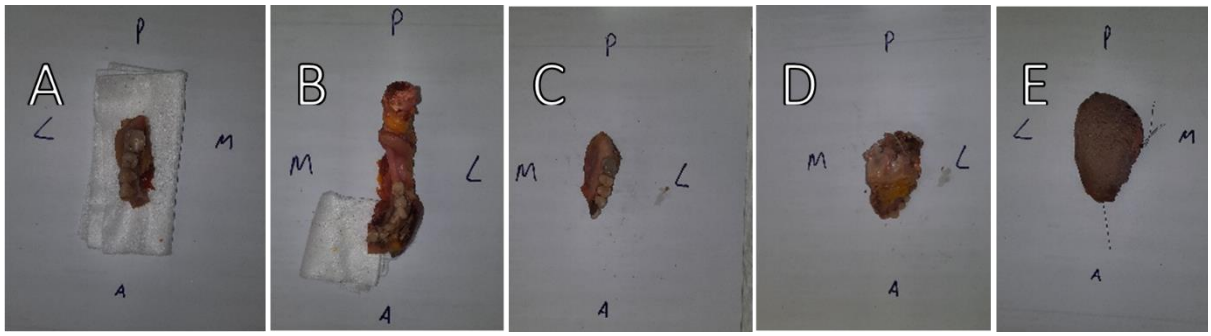

Figure 4: Regular photography of resection specimen from human cadaveric head taken directly after resection. Annotated in frame with "A" for anterior, "P" for posterior, "M" for medial and "L" for lateral. A) Partial mandibulectomy, held upright by a piece of gauze. B) Hemimandibulectomy held upright by a piece of gauze. C) Maxillectomy. D) Maxillectomy including orbita floor. E) Tongue section.

After resection, the specimens were scanned once with each scanner. This was done at ambient light. The specimens were placed on a matte sheet of plastic (Figure 5) for the EinScan SP, the EinScan H2 and the Einstar, as these scanners have a large field of view (FOV) and cannot have other objects in the frame. The matte black sheet also ensures there is little reflection from the surface surrounding the specimen and allows for an ease in clean up after the scan has been completed. In the case of the TRIOS iOS the specimen was scanned freehand, as it has smaller FOV, ensuring the hands and fingers of the operator are never in frame while giving more degrees of freedom and an easier scanning procedure.

Figure 5: Cadaveric maxilla specimen on a sheet of matte black plastic ready for scanning. Here placed on top of the turntable of the EinScan SP.

For scans made with the H2 and Einstar, reflective markers provided with the scanners were used on the sheet of matte plastic to help the scanner maintain orientation during the scans, as show in Figure 6.

Figure 6: Cadaveric specimen of the partial mandibulectomy place atop of a sheet of matte black plastic with reflective markers added in preparation of scanning with the H2 and Einstar.

After scanning, the models were processed in the software provided with each respective scanner to create stereolithography files (.stl), a filetype that uses triangles to represent the surface of a 3D object.

For the second comparison, two 3D prints were created , one of an abstracted model of a dental inlay and one of a crown and bridge, they are shown in Figure 7. The design of these models was based on from ISO standard 12836-2015 and was discussed in the feasibility study. The design drawings can be found in Appendix B and Appendix C

. To ensure the 3D prints themselves were accurate to the design they were each printed 5 times on two different 3D printers, the NextDent5100 and the Formlabs available on the RadboudUMC 3DLab. In turn, the prints were each measured 5 times with a pair of digital vernier callipers with 0.01mm accuracy. In doing so, the random errors introduced via the

printing process and user measurements were reduced. The exact process for these calliper measurements of the 3D prints is depicted in Appendix D.

From these 3D prints, the ones with the most accurate dimensions, as compared to the design, were selected for scanning. The assumption was made that if the measured dimensions are accurate, the rest of the model's shape would also be accurate and be most suited for the 3D scanner comparison. The chosen 3D prints were then each scanned 5 times with each 3D scanner, again in an attempt to reduce the random errors.

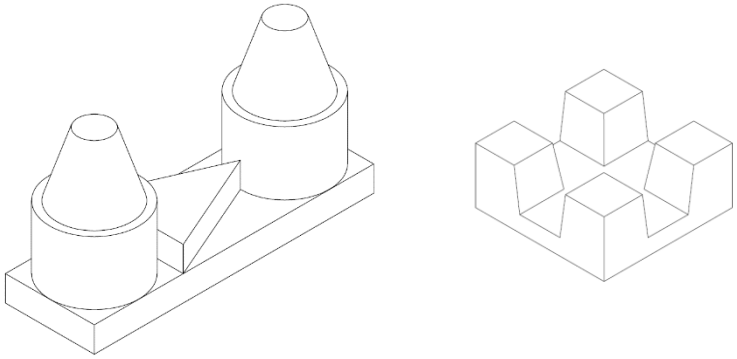

Figure 7: Schematics of the two 3D print designs used in the scanner comparison research Left: Crown and bridge model. Right: Inlay model

The reference CT-scan of the cadaveric head was created prior to resection, on the Radboud UMC radiology department. A 3D model of this CT scan was then created in 3D Slicer, a freeware software for radiography image processing (40).

The results of the four scanners were then analysed. The 3D models of the cadaveric specimens were used to create and compare distance maps with the CT derived model in 3DMedX® (v1.2.35.0, Radboudumc, Nijmegen, The Netherlands). Furthermore, scanner time and ease of use were compared.

In the case of the 3D printed models, the dimensions of the scans were measured in Blender (41), a 3D design program, as this provides tools to easily measure geometric shapes. These measurements were then compared to those obtained with the vernier callipers.

Results

Vernier callipers

The results of the measurements with the vernier callipers of the most accurately 3D printed models, one of each type, can be seen in Table 1. These models best matched the actual dimensions of the design and were chosen as the 3D models to be scanned.

Table 1: Measurements of the 3D printed inlay, and crown and bridge models. Performed with digital vernier callipers. Measurements in millimetres. In the left column the dimensions as determined in the 3D design are shown in parenthesis.

inlay model	Mean	mean error	SD	mean error %
measurepoint 1 (sides 16mm)	16.00	0.00	0.01	0.02
measurepoint 2 (height 7mm)	6.89	-0.11	0.04	1.61
measurepoint 3 (inner cut (5mm)	5.10	0.10	0.02	2.06
measurepoint 4 (lower plane height)	2.08	0.08	0.04	3.90
measurepoint 5 (depth 5mm)	4.92	-0.08	0.01	1.53
crown and bridge	**Mean**	**mean error**	**SD**	**mean error %**
measurepoint 1 (lower plane 4mm)	3.89	-0.11	0.04	2.85
measurepoint 2 (middle plane 8mm)	7.87	-0.13	0.02	1.58
measurepoint 3 (upper middle plane 14mm)	13.69	-0.31	0.02	2.24
measurepoint 4 (max height 24mm)	23.52	-0.48	0.03	1.99
measurepoint 5 (width 14mm)	14.04	0.04	0.04	0.30
measurepoint 6 (length 44mm)	44.11	0.11	0.05	0.25
measurepoint 7 (height tower 10mm)	9.75	-0.25	0.02	2.49

3D prints

The 3D prints were scanned with all four scanners, neither the H2 nor the Einstar could gather sufficient data of these relatively small 3D prints to generate any 3D models, as such no results were generated for these two scanners with regard to scanning the 3D printed models.

The iOS and EinScan SP could scan the 3D prints and were successfully used to scan both printed models 5 times each. The same dimensions as measured with the callipers were

then measured on the 3D digital models using Blender. The results of the measurements can be seen in

Table 2 for the iOS and

Table 3 for the EinScan SP.

For the inlay model the iOS was accurate within an average of 0.03mm across all measured dimensions (an error of 0.88% with standard deviations ranging from 0 to 0.05) and the Einscan was accurate within an average of 0.07mm (an error of 1.32% with standard deviations ranging from 0.05 to 0.10). For the crown and bridge model the iOS was accurate within an average of 0.12mm across all measured dimensions (an error of 1.03% with standard deviations ranging from 0 to 0.05) and the EinScan SP was accurate within an average of 0.12mm (an error of 1.19% with standard deviations ranging from 0.0 to 0.20). In none of the measurements was the difference between the iOS and EinScan SP measurement greater than 0.4mm.

Visual inspection of the digital scans does seem to show a less homogenous surface for the EinScan SP models compared to the iOS models which is illustrated in Figure 8, indicating that the iOS is better able to pick-up small-scale details.

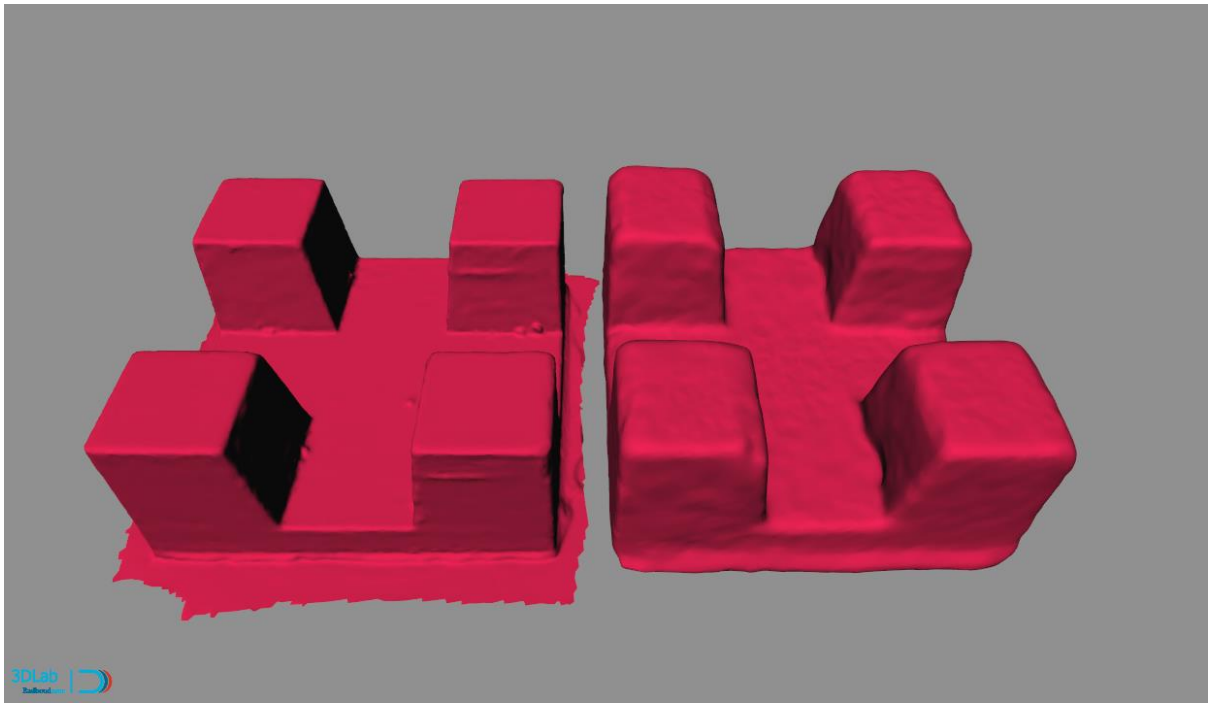

Figure 8: 3D digital models of the inlay 3D prin. On the left the model created with the TRIOS iOS scan, on the right the model created with the EinScan SP

Table 2: Measurements of the inlay and crown and bridge 3D digital models created with the iOS as measured in Blender. In the left column the actual dimension of the models, as measured with vernier callipers, are notated in parenthesis.

inlay model	Mean	mean error	SD	mean error %	Mean of errors
measurepoint 1 (sides 16mm)	15.98	-0.02	0.00	0.16	
measurepoint 2 (height 6.89mm)	6.93	0.04	0.00	0.57	
measurepoint 3 (inner cut 5.10mm)	5.14	0.04	0.01	0.80	
measurepoint 4 (lower plane height 2.08mm)	2.03	-0.06	0.04	2.75	
measurepoint 5 (depth 4.92mm)	4.93	0.00	0.04	0.10	0.03
crown and bridge	Mean	mean error	SD	mean error %	Mean of errors
measurepoint 1 (lower plane 3.89mm)	4.01	0.12	0.02	3.00	
measurepoint 2 (middle plane 7.87mm)	7.94	0.07	0.05	0.81	
measurepoint 3 (upper middle plane 13.69mm)	13.83	0.14	0.04	0.96	
measurepoint 4 (max height 23.52mm)	23.92	0.40	0.04	1.65	
measurepoint 5 (width 14.04mm)	13.98	-0.06	0.02	0.43	
measurepoint 6 (length 44.11mm)	44.15	0.04	0.02	0.09	
measurepoint 7 (height tower 9.75mm)	9.78	0.02	0.00	0.25	0.12

Table 3: Measurements of the inlay and crown and bridge 3D digital models created with the EinScan SP as measured in Blender. In the left column the actual dimension of the models, as measured with vernier callipers, are notated in parenthesis.

inlay model 2	Mean	mean error	SD	mean error %	Mean of errors
measurepoint 1 (sides 16mm)	16.07	0.07	0.08	0.44	
measurepoint 2 (height 6.89mm)	6.80	-0.09	0.05	1.36	
measurepoint 3 (inner cut 5.10mm)	5.07	-0.03	0.06	0.60	
measurepoint 4 (lower plane height 2.08mm)	2.03	-0.05	0.10	2.50	
measurepoint 5 (depth 4.92mm)	5.01	0.09	0.09	1.70	0.07
crown and bridge 2	Mean	mean error	SD	mean error %	
measurepoint 1 (lower plane 3.89mm)	4.03	0.14	0.20	3.38	
measurepoint 2 (middle plane 7.87mm)	7.92	0.05	0.14	0.62	
measurepoint 3 (upper middle plane 13.69mm)	13.78	0.09	0.15	0.61	
measurepoint 4 (max height 23.52mm)	23.81	0.29	0.03	1.21	
measurepoint 5 (width 14.04mm)	14.15	0.11	0.01	0.79	
measurepoint 6 (length 44.11mm)	44.14	0.03	0.09	0.07	
measurepoint 7 (height tower 9.75mm)	9.92	0.16	0.00	1.65	0.12

Cadaveric specimen

In the case of the cadaveric specimen both the H2 as the Einstar again failed to gather enough data to scan the specimens, as such here too no results were produced for these two scanners. The iOS and the EinScan SP however produced successful 3D models of the specimens. Using 3DMedX the 3D models were registered onto a model of the skull, which itself was generated in 3DMedX as well. The resultant models can be seen in Figure 9 and Figure 10. Note the colour of the iOS, which produced artifacts in both colour and form of the texture. The EinScan SP scans have a truer to life colour representation. The specimen of the tongue , while successfully scanned, could not be accurately placed within the CT scan, so its models were not used for the results.

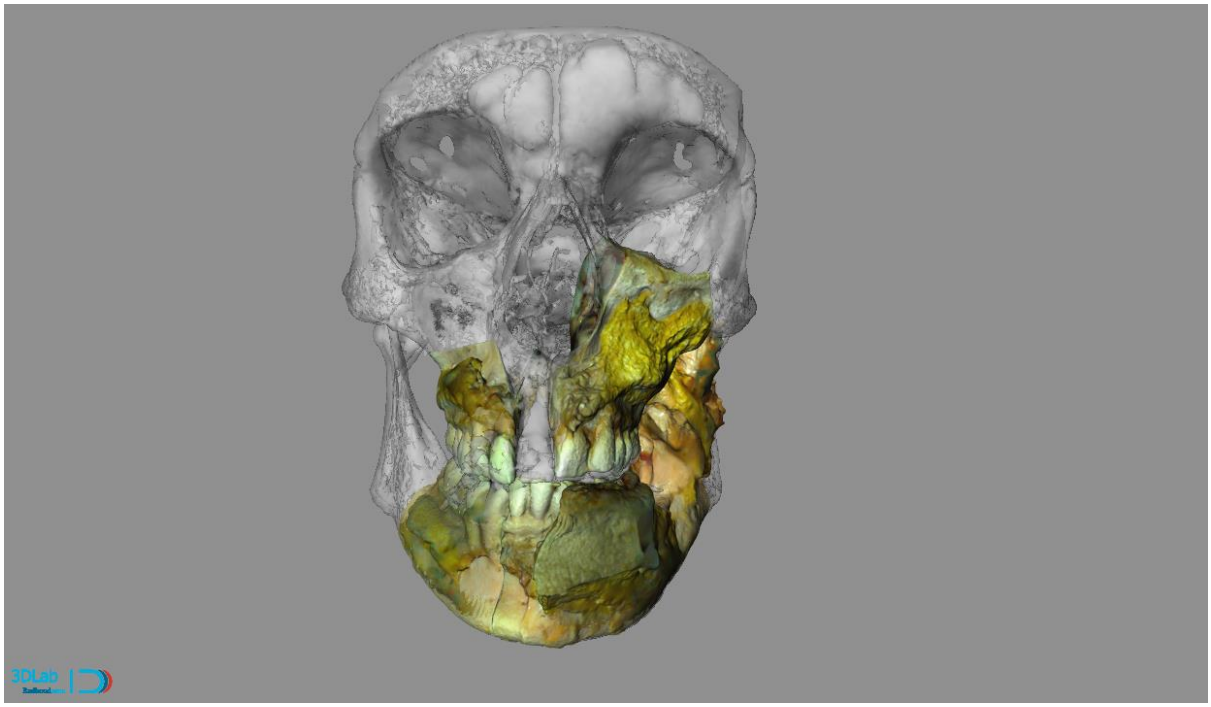

Figure 9: 3D models of the five cadaveric specimens created with the EinScan SP registered onto the reference CT.

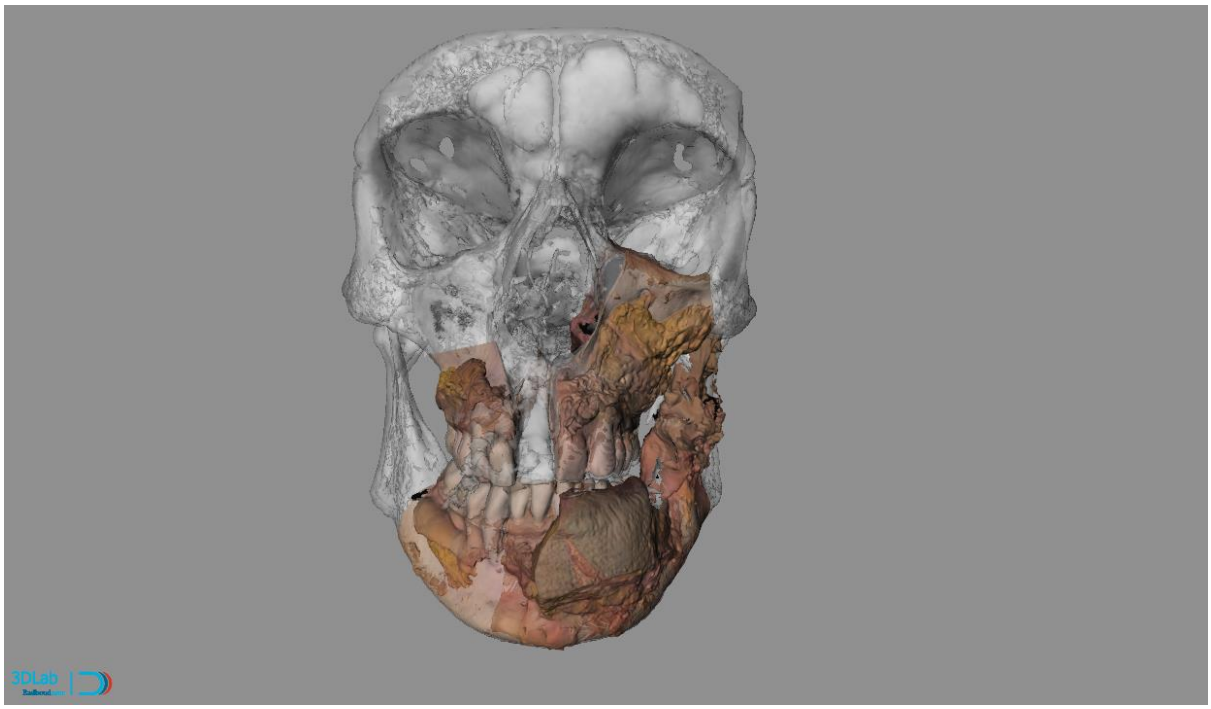

Figure 10: 3D models of the five cadaveric specimens created with the TRIOS iOS registered onto the reference CT.

Distance maps created for each set of scans showed a deviation of +/- 2mm on the bony structures. This was true for both the iOS scans as the EinScan SP scans. Soft tissue, being absent on the CT, was not considered for this. The time per scan can be found in Table 4, the EinScan SP required an average of 3:55 minutes to complete a scan (range: 3:37-4:50), for the iOS this was an average of 5:24 minutes (range: 3:44-6:12). The ease of use was recorded by a single operator using a system useability scale (SUS) questionnaire, which can be found in Appendix E. The results of this questionnaire were that the EinsScan SP was the preferred scanner, mainly because the iOS is an entirely manual process, whereas the EinScan SP is a "hands-off" system; once the scanning start no user input or handling is required.

Table 4: Scan times for each of the five specimens, recorded for the EinScan SP and TRIOS iOS.

	EinScan SP	TRIOS iOS
Specimen A	03:43	04:16
Specimen B	03:42	06:12
Specimen C	03:45	06:11
Specimen D	03:37	03:44
Specimen E	04:50	06:37
Average	03:55	05:24

Conclusion

The results indicate that the H2 and Einstar are not suitable for scanning (human tissue) at this scale. The iOS was found to be more accurate than the EinScan SP and have a higher trueness, as indicated by its lower deviation across repeated measurements of the same objects and the distance maps generated to visualize this. The difference is however relatively small, with both scanners being accurate within 1-2% of the actual dimensions.

The difference in ease of use and time to scan is where the two scanners differ most, the Einscan has a higher ease of with the "hands off" automatic turntable, this also facilitates a reduced time to scan. In the setting of scanning human tissue the EinScan SP was ultimately found to be superior. However, in cases where repeatability or extremely high precision are of importance, the iOS could be considered worth the extra scan time.

4

Improving the Scanning Workflow

Another aspect set out to improve was the scanning workflow. Previous research into creating 3D models had established a workflow with the TRIOS iOS which worked within the scope of scanning human tissue. As the scanner of choice became the EinScan SP after the scanner comparison research, an adapted workflow was required. Contact was sought with dr. Michael Topf , who is the corresponding author of several papers, which detail the use of the EinScan SP to scan human resection specimens. Dr. Topf and his research team were very generous in both their availability (through Teams sessions) and subsequent shared insights into their workflow, scanning process and use of the EinScan SP.

This resulted in not only a better understanding of how to use the EinScan SP in the future, but also in the creation of a manual to help any further research with the EinScan SP with regard to scanning human tissue. The manual is in Dutch to ensure broader usability within the Radboud UMC and may be found in Appendix F.

5

Integration of Histopathology

Introduction

A further goal of this master thesis project was to include histopathological information into 3D models of the resection specimen. During the second year of the master internship, research was conducted into creating 3D models of the resection specimen, and integrating them into the CT images. This process is therefore not detailed in this part of the report, instead the title page of a document with details regarding the process can be found in Appendix G and can be shared upon request. This document includes information on how to scan human tissue with the iOS and alignment of the resultant models on CT images). Instead, the focus is entirely on of how histopathological images and information were integrated into a resection specimen 3D model.

Method

A single patient case was selected to determine a method by which to include histopathological information. The patient had undergone a hemimandibulectomy for an oral SCC, after which they received adjuvant radiotherapy. The resection specimen was in this case still scanned with the iOS, as the EinScan SP was still under review in the scanner comparison research. The resection specimen 3D model was registered onto CT data, which can be seen in Figure 11.

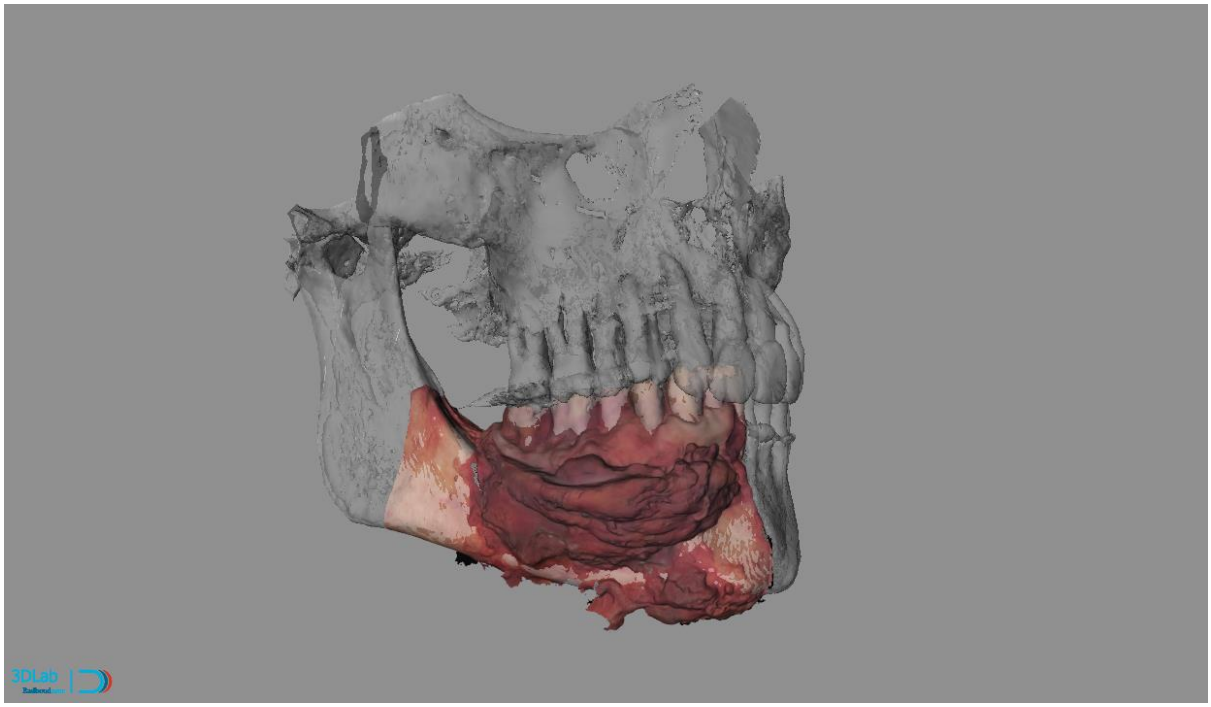

Figure 11: Resection specimen of patient who had undergone a hemimandibulectomy registered onto its correct location on a model derived from a preoperative CT.

Gross sectioning histopathology images were taken from the RadboudUMC pathology database. Using GIMP, an image editor, their contours were extracted as .png masks and numbered in order from anterior to posterior, this numbering was maintained throughout the process. The gross sections and their contouring can be seen in Figure 12.

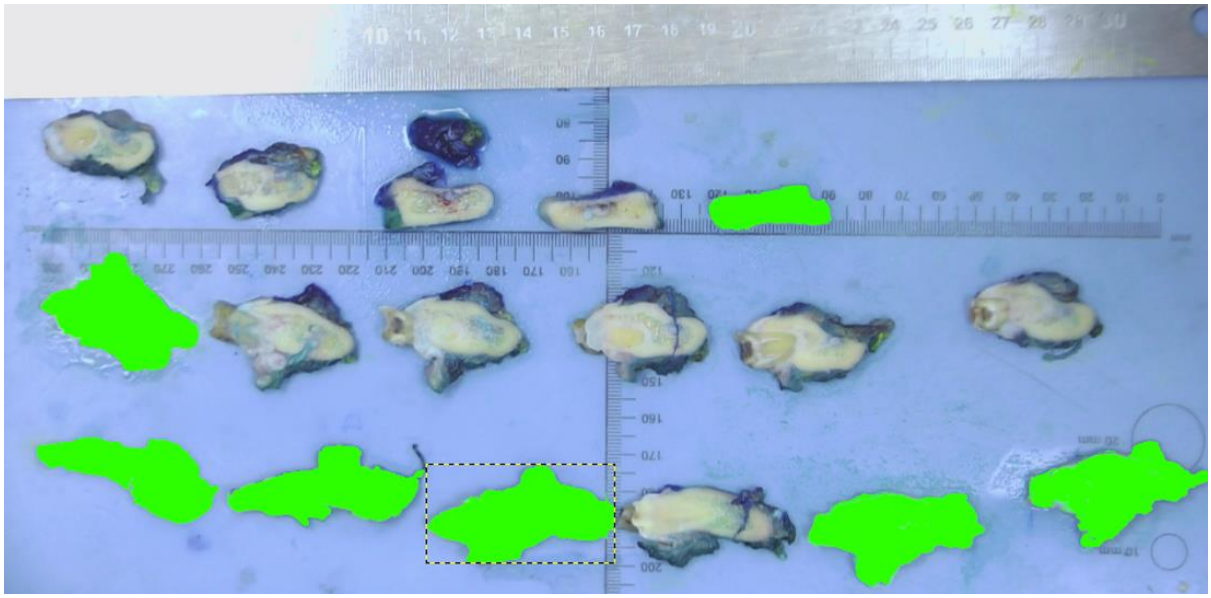

Figure 12: Photo from the pathology database of all gross section slices from the hemimandibulectomy patient. In green are the contour masks generated in GIMP.

The .png masks were then imported into InkScape, a vector graphics program, in which the .png files of the contours were converted into .svg vector graphics. The vector graphics could then be loaded into Blender, a 3D design program, wherein the vector graphics were in turn converted into .stl 3D models with a certain thickness and given correct dimensions in accordance with the histopathology images. To determine this thickness, the length of the resection specimen was measured in 3DMedX and divided by the number of gross section slices, resulting in the average thickness each slice needed to be.

The 3D models of the gross sections were loaded into 3DMedX together with the CT registered/aligned 3D model of the resection specimen. The gross section 3D models were first aligned by eye on their correct locations withing the resection specimen, using the numbering to maintain their correct order. After this manual alignment, an iterative closest point registration (ICP) was performed to achieve an alignment for each gross section with the model. Only the edges of the gross section models were used, as the anterior and posterior surface area of each gross section 3D model is not included in the resection specimen 3D model (as this has not been cut). However, the edges of the gross sections 3D models are generated by

simply giving them a thickness in Blender, these edges do not contain accurate details matching that of the resection specimen model. As such, the registration is an approximation.

After registration, all slices and the resection specimen models were loaded into 3D Slicer. The written pathology report was then used to segment and annotate areas of interest in the 3D model, specifically the gross section slices which showed tumour involvement, and the irradical margins. The pathology report included information relating findings to gross section slice count, anatomic orientation (medial, lateral, caudal, cranial) and measurements regarding margins accurate up to 0.1mm. The locations were ultimately segmented from the 3D model of the resection specimen, guided by the pathology report and 3D models of the gross sections.

Results

The resulting 3D model includes all gross section slices , annotated by colour, in their most optimal position and can be seen in Figure 13. The inaccuracies introduced by translating 2D photography into a 3D model are clearly visible. Figure 14 shows the final position of the reported irradical margins. Of note, is that the scale of the gross sections does not seem to match that off the resection specimen, possibly caused by changes in shape and size of the specimen, between the moment of resection and the moment of gross sectioning.

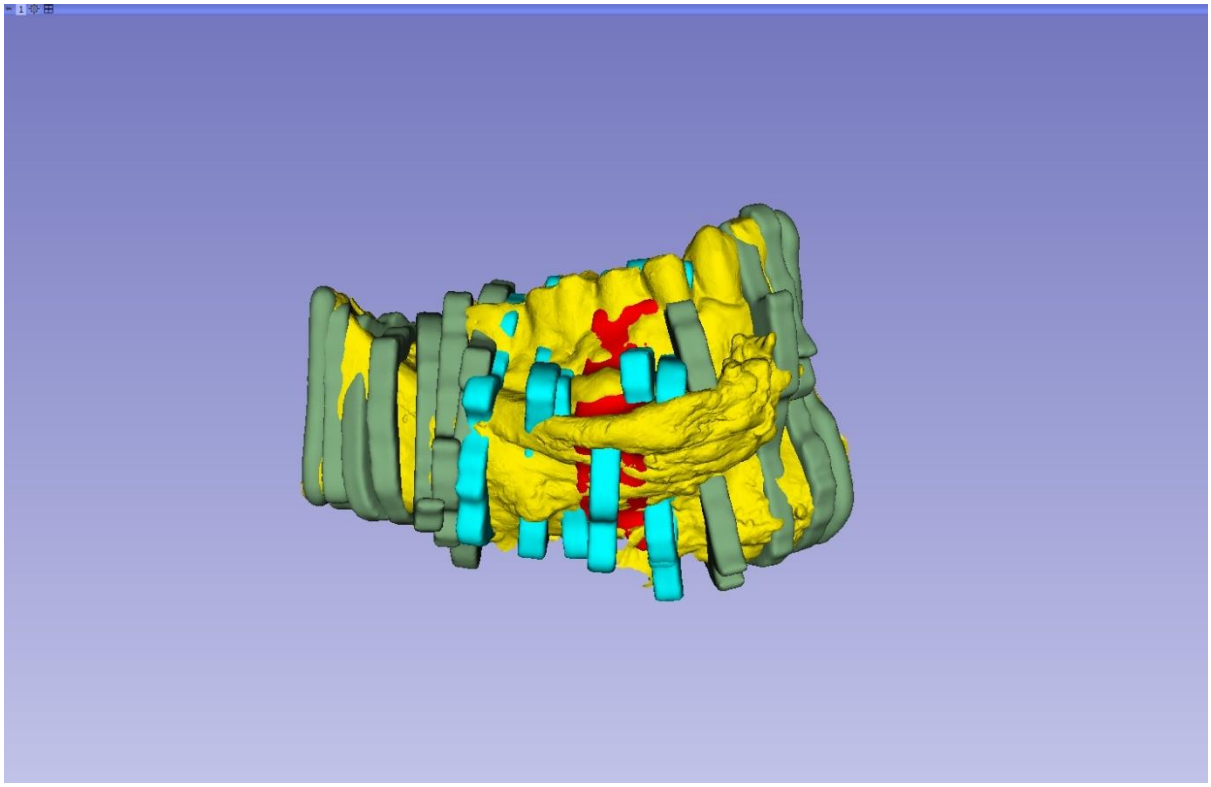

Figure 13: 3D model shown in 3D slicer. In yellow the model of the resected mandible. In green the gross section slice models generated in Blender. In turquoise the gross section with tumour involvement. In red the irradical margin as reported in the written pathology report.

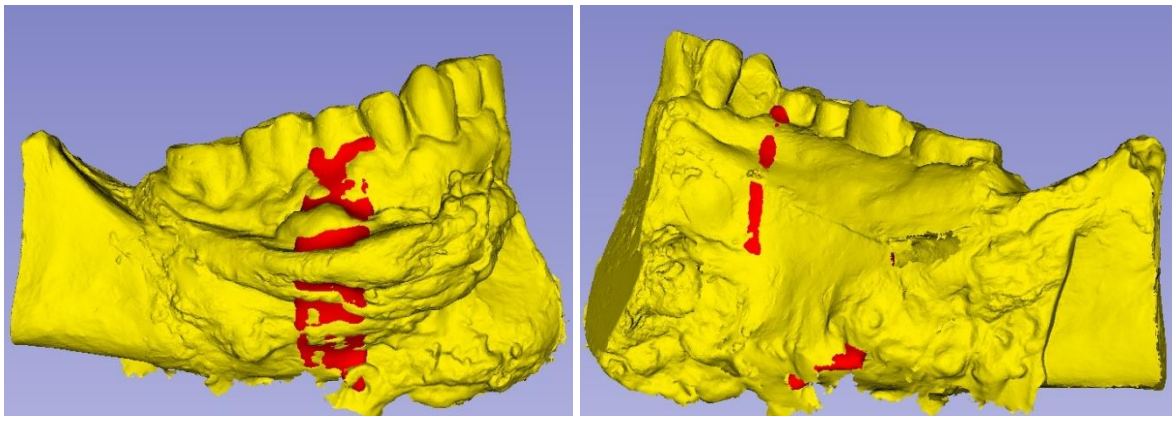

Figure 14: 3D model shown in 3D slicer. In yellow the model of the resected mandible. In red the irradical margin as reported in the written pathology report.

6

Use Case in Adjuvant Radiotherapy

Introduction

The goal of the 3D models is to have a clinical impact. To achieve this the RadboudUMC radiotherapy department was approached for possibilities to collaborate. After consulting with several experts from their department, and having experienced the overall workflow over the course of several days, it became clear that the 3D models with histopathology integration could, in principle, be of use to the radiotherapy team during the creation radiotherapy treatment plans.

Method

The same patient case, as for the histopathologic data integration was selected, as this patient had already undergone adjuvant radiotherapy, and therefore a preexisting radiotherapy plan and a (post operative) pre-radiotherapy planning CT were available, which could be overlaid and compared to the 3D model matched onto the pre-operative CT.

The resultant models from the histopathology integration were .stl files. For the radiotherapy team to be able to use these models, they first needed to be converted from .stl into RT-struct files. The radiation treatment planning software used by the radiotherapy team at the RadboudUMC consists of Siemens Pinnacle(42). This software cannot read .stl files and must have segmentation or contours offered to it in the legacy RT struct format. Complex geometric .stl files or multi-object segmentations, cannot be (reliably) converted into RT-struct files. As such all the models first had to be simplified. This was achieved in 3D-Slicer by first converting each .stl file into a segmentation, then reducing each segmentation to its single largest object (although, for the gross section models, and models of margin status, this was

already the case), and then smoothing the segmentations, the result can be seen in Figure 15. All segmentations, together with the preoperative CT, were then exported using 3D Slicer's radiation planning module as a DICOM file with all segmentations contained within as RT structs. This DICOM was sent to the radiotherapy team, which could then successfully load it into Pinnacle.

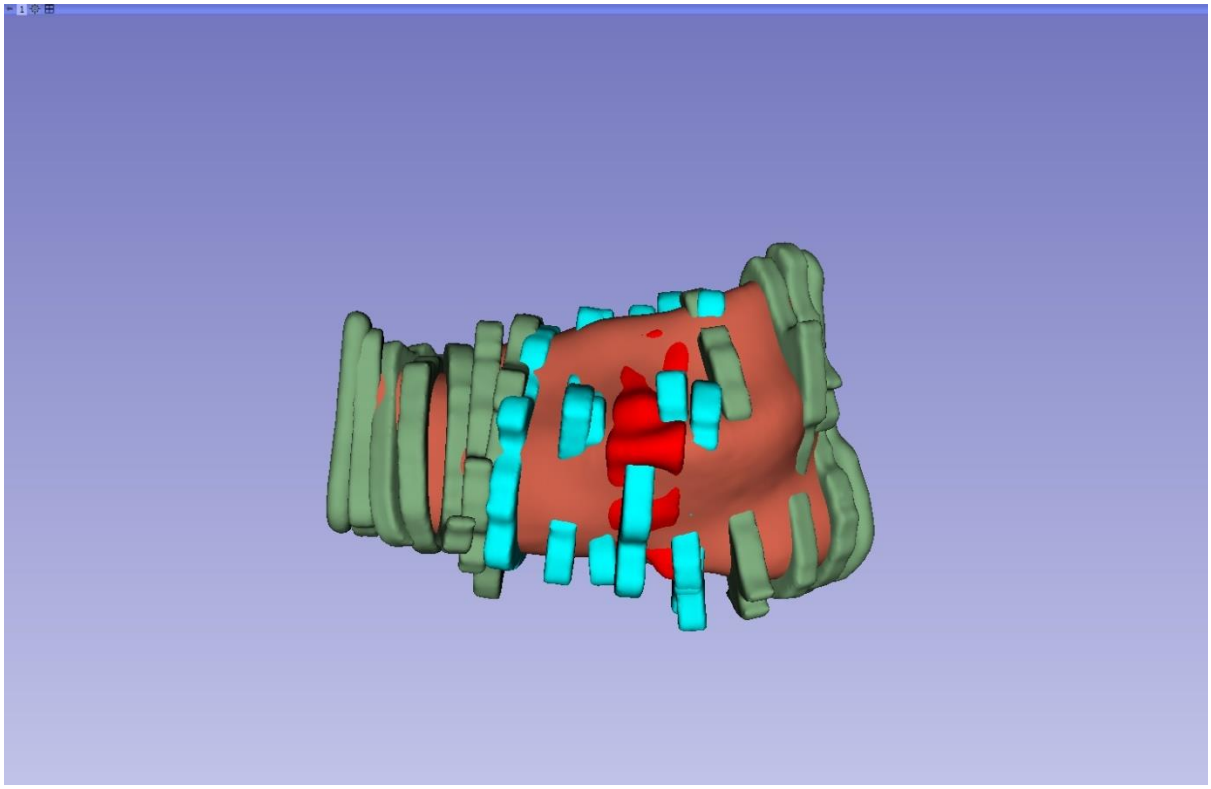

Figure 15: The smoothed 3D model shown in 3D slicer ready for export as RT struct files. In light red the smoothed resected mandible. In green the smoothed gross section slice models. In turquoise the smoothed gross sections with tumour involvement. In red the irradical margin as reported in the written pathology report, this required no further smoothing.

In Pinnacle the preoperative scan was registered onto the post operative radiation treatment planning CT, and the same transformations were applied to all the gross section segmentations, aligning all the segmentations to the planning CT.

Results

Due to the post operative situation being different to the preoperative situation (the mandibula had been replaced with a free fibula flap), alignment of the two CTs with a rigid registration was an approximation.

Two experts from the radiotherapy department analysed the radiation treatment planning-CT *with* the added segmentations of the gross sections and radical margin. They overlaid the performed radiation plan (see Figure 16) and, assuming the locations of the segmentations were depicted accurately, concluded that a dose volume reduction would have been possible with the additional visualized histopathologic findings regarding the location of irradical margins.

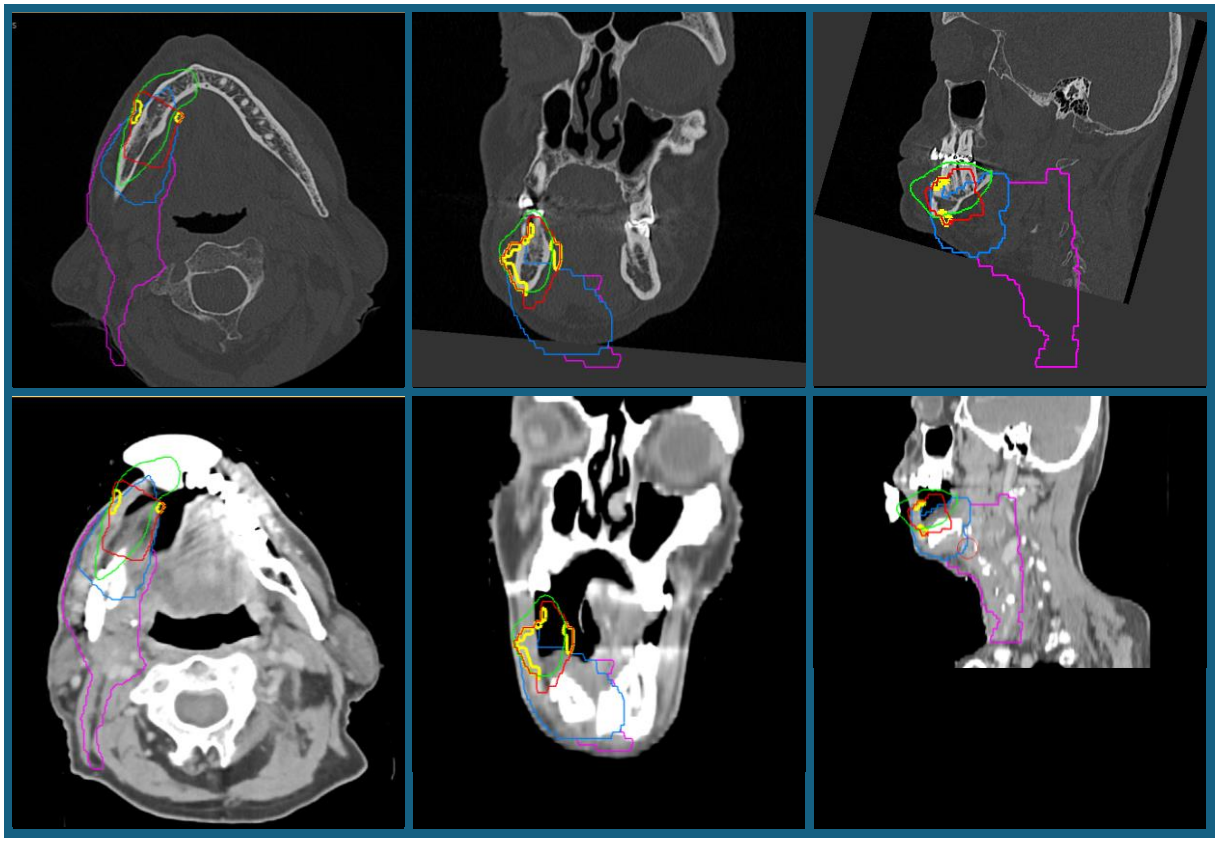

Figure 16: The segmentations of the resected mandible (green contour), affected gross section slices (red contour) and radical margins (yellow margins) placed in the preoperative CT scan (top row: axial, coronal and sagittal respectively) and then registered/matched onto the post operative radiotherapy planning CT (bottom row: axial, coronal and sagittal respectively). Projected on both is the performed radiotherapy plan's CTV (purple contour) and GTV (blue contour). The top and bottom row show CT at corresponding levels of both scans.

Furthermore, both experts were of the opinion, that even in absence of millimetre accuracy of the segmentations' location, the information would, in of itself, be of added value to the decision making during planning, and separate to loading the information into their planning software Pinnacle.

7

General discussion and conclusion

The 3D models with histopathological inclusion created during this project are very promising. The EinScan SP is a capable scanner which manages to scan sufficiently detailed and accurate models of resection specimens.

The use of 2D photography to recreate the 3D structure of the gross sections however leaves much to be desired, not only are they not an accurate representation of reality, but the workflow also requires knowledge of a plethora of software suits. This makes the process is both time consuming and cumbersome to work with. During the course of this research possibilities were explored to scan the gross sections directly on the pathology department, rather than turning contours into 3D models. This was in principle successful with the pathology department being enthusiastic about the possibilities of 3D scanning gross sections. This, however, did not yet produce useable results due to the limited opportunity which was had so far to create such scans. In the future however it is desirable to pursue this further to have accurate 3D models of the gross sections. This will be useful to have a digital record of the gross sections (which are currently stored in freezers) and make the 3D models easier to register on the correct location in the resection specimen.

The results of the radiotherapy are encouraging, but very much still in their infancy. There is currently no validation that the position of the resection specimens in the CT are correct, nor of the placement of the gross section models. While this was not the goal of this research it is something that should be pursued in future research. Furthermore, registration of the preoperative CT scans onto the postoperative planning CT scans could benefit from exploring possibilities of non-rigid registration to place the resection specimen and margins more accurately in the postoperative situation.

Conclusion

This research successfully created a first 3D model of resection specimens, registered onto CT scan derived models, and enhanced with histopathological information such as non-free margins. The radiotherapy team judged this model as promising for planning radiation therapy, noting its potential to improve the precision of treatment delivery. By incorporating detailed histopathological information, the model allowed for a more accurate delineation of tumour boundaries and critical margins, thus having potential to facilitate targeted radiation while minimizing exposure to healthy tissues. This integration could represent enhance radiotherapy planning and help deliver more personalized cancer treatment outcomes.

References

1. Bray F, Laversanne M, Sung H, Ferlay J, Siegel RL, Soerjomataram I, et al. Global cancer statistics 2022: GLOBOCAN estimates of incidence and mortality worldwide for 36 cancers in 185 countries. CA Cancer J Clin. 2024;74(3):229-63.

2. Parkin DM, Bray F, Ferlay J, Pisani P. Global cancer statistics, 2002. CA Cancer J Clin. 2005;55(2):74-108.

3. Miguelanez-Medran BC, Pozo-Kreilinger JJ, Cebrian-Carretero JL, Martinez-Garcia MA, Lopez-Sanchez AF. Oral squamous cell carcinoma of tongue: Histological risk assessment. A pilot study. Med Oral Patol Oral Cir Bucal. 2019;24(5):e603-e9.

4. Chamoli A, Gosavi AS, Shirwadkar UP, Wangdale KV, Behera SK, Kurrey NK, et al. Overview of oral cavity squamous cell carcinoma: Risk factors, mechanisms, and diagnostics. Oral Oncol. 2021;121:105451.

5. Kumar M, Nanavati R, Modi TG, Dobariya C. Oral cancer: Etiology and risk factors: A review. J Cancer Res Ther. 2016;12(2):458-63.

6. 1. Mouth and oral cancer statistics. 2022. 2022 [cited 2024. Available from: https://www.wcrf.org/cancer-trends/mouth-and-oral-cancer-statistics/

7. Montero PH, Patel SG. Cancer of the oral cavity. Surg Oncol Clin N Am. 2015;24(3):491-508.

8. Neville BW, Day TA. Oral cancer and precancerous lesions. CA Cancer J Clin. 2002;52(4):195-215.

9. Waldron CA, Shafer WG. Leukoplakia revisited. A clinicopathologic study 3256 oral leukoplakias. Cancer. 1975;36(4):1386-92.

10. Shafer WG, Waldron CA. Erythroplakia of the oral cavity. Cancer. 1975;36(3):1021-8.

11. Hosni A, Chiu K, Huang SH, Xu W, Huang J, Bayley A, et al. Non-operative management for oral cavity carcinoma: Definitive radiation therapy as a potential alternative treatment approach. Radiother Oncol. 2021;154:70-5.

12. Forner D, Noel CW, Wu V, Parmar A, Chan KKW, de Almeida JR, et al. Nonsurgical management of resectable oral cavity cancer in the wake of COVID-19: A rapid review and meta-analysis. Oral Oncol. 2020;109:104849.

13. Subramaniam SS, Paterson C, McCaul JA. Immunotherapy in the management of squamous cell carcinoma of the head and neck. Br J Oral Maxillofac Surg. 2019;57(10):957-66.

14. Cancer stat facts: oral cavity and pharynx cancer.: National Cancer Institute; 2024 [Available from: https://seer.cancer.gov/statfacts/html/oralcav.html.

15. Amit M, Yen TC, Liao CT, Chaturvedi P, Agarwal JP, Kowalski LP, et al. Improvement in survival of patients with oral cavity squamous cell carcinoma: An international collaborative study. Cancer. 2013;119(24):4242-8.

16. Chinn SB, Myers JN. Oral Cavity Carcinoma: Current Management, Controversies, and Future Directions. J Clin Oncol. 2015;33(29):3269-76.

17. Boysen M, Lovdal O, Tausjo J, Winther F. The value of follow-up in patients treated for squamous cell carcinoma of the head and neck. Eur J Cancer. 1992;28(2-3):426-30.

18. Blatt S, Kruger M, Sagheb K, Barth M, Kammerer PW, Al-Nawas B, et al. Tumor Recurrence and Follow-Up Intervals in Oral Squamous Cell Carcinoma. J Clin Med. 2022;11(23).

19. Frauenfelder C, Shelmerdine SC, Simcock IC, Hall A, Hutchinson JC, Ashworth MT, et al. Micro-CT Imaging of Pediatric Thyroglossal Duct Cysts: A Prospective Case Series. Front Pediatr. 2021;9:746010.

20. Eberspacher-Schweda MC, Schmitt K, Handschuh S, Fuchs-Baumgartinger A, Reiter AM. Diagnostic Yield of Micro-Computed Tomography (micro-CT) Versus Histopathology of a Canine Oral Fibrosarcoma. J Vet Dent. 2020;37(1):14-21.

21. Necker FN, Chang M, Leuze C, Topf MC, Daniel BL, Baik FM. Virtual Resection Specimen Interaction Using Augmented Reality Holograms to Guide Margin Communication and Flap Sizing. Otolaryngol Head Neck Surg. 2023;169(4):1083-5.

22. Deferm JT, Schreurs R, Baan F, Bruggink R, Merkx MAW, Xi T, et al. Validation of 3D documentation of palatal soft tissue shape, color, and irregularity with intraoral scanning. Clinical Oral Investigations. 2017;22(3):1303-9.

23. Radonic T, Dickhoff C, Mino-Kenudson M, Lely R, Paul R, Thunnissen E. Gross handling of pulmonary resection specimen: maintaining the 3-dimensional orientation. J Thorac Dis. 2019;11(Suppl 1):S37-S44.

24. Meulemans J, Narimani S, Hauben E, Nuyts S, Laenen A, Delaere P, et al. Introduction of a New Pathology Workup Protocol for Glottic Cancer Treated With Transoral Laser Microsurgery (TLM): Prospective Analysis of Oncological Outcomes and Matched Case-Control Study. Front Oncol. 2021;11:685255.

25. Meulemans J, Hauben E, Peeperkorn S, Nuyts S, Delaere P, Vander Poorten V. Transoral Laser Microsurgery (TLM) for Glottic Cancer: Prospective Assessment of a New Pathology Workup Protocol. Front Surg. 2020;7:56.

26. Mahmoud A, Bennett M. Introducing 3-Dimensional Printing of a Human Anatomic Pathology Specimen: Potential Benefits for Undergraduate and Postgraduate Education and Anatomic Pathology Practice. Arch Pathol Lab Med. 2015;139(8):1048-51.

27. Miller A, Prasad K, Sharif KF, Adams DJ, Garbow L, Roberts E, et al. Virtual 3D Specimen Mapping in Head & Neck Oncologic Surgery. Laryngoscope. 2023.

28. Sharif KF, Perez AN, Sharbel DD, Griffith B, Pruthi S, Rohde SL, et al. Multimodal Virtual 3D Representation of a Giant Cell Tumor of the Thyroid Cartilage. Ear Nose Throat J. 2022:1455613221091090.

29. Sharif KF, Prasad K, Miller A, McPeak S, Denney JE, Lewis JS, Jr., et al. Enhanced Intraoperative Communication of Tumor Margins Using 3D Scanning and Mapping: The Computer-Aided Design Margin. Laryngoscope. 2023;133(8):1914-8.

30. Sharif KF, Lewis JS, Jr., Ely KA, Mehrad M, Pruthi S, Netterville JL, et al. The computer-aided design margin: Ex vivo 3D specimen mapping to improve communication between surgeons and pathologists. Head Neck. 2023;45(1):22-31.

31. Aaboubout Y, Barroso EM, Algoe M, Ewing-Graham PC, Ten Hove I, Mast H, et al. Intraoperative Assessment of Resection Margins in Oral Cavity Cancer: This is the Way. J Vis Exp. 2021(171).

32. Perez AN, Sharif KF, Guelfi E, Li S, Miller A, Prasad K, et al. Ex vivo 3D scanning and specimen mapping in anatomic pathology. J Pathol Inform. 2023;14:100186.

33. Saturno MP, Brandwein-Weber M, Greenberg L, Silberzweig A, Buchbinder D, Dowling EM, et al. Utilizing 3D head and neck specimen scanning for intraoperative margin discussions: Proof of concept of our novel approach. Head and Neck-Journal for the Sciences and Specialties of the Head and Neck. 2023;45(1):10-21.

34. Koivuholma A, Aro K, Mäkitie A, Salmi M, Mirtti T, Hagström J, et al. Three-Dimensional Presentation of Tumor Histopathology: A Model Using Tongue Squamous Cell Carcinoma. Diagnostics (Basel). 2021;11(1).

35. EinScan SP Specs 2024 [Available from: https://www.einscan.com/einscan-sp/einscan-sp-specs/.

36. EinScan H2 Specs 2024 [Available from: https://www.einscan.com/handheld-3d-scanner/einscan-h/einscan-h2-specs/.

37. EINSTAR 3D Scanner 2024 [Available from: https://www.crea3d.com/en/handheld-3d-scanners/1072-einstar-3d-scanner.html.

38. TRIOS 3 2024 [Available from: https://www.tdentallab.com/trios/trios-3/.

39. -. Dissection rooms

D.E. Doomernik, MD (Head dissection rooms) Department of Medical Imaging, Anatomy

Radboud University Medical Center

Postbus 9101, 6500 HB Nijmegen, The Netherlands (route 102)

www.radboudumc.nl

40. Fedorov A, Beichel R, Kalpathy-Cramer J, Finet J, Fillion-Robin JC, Pujol S, et al. 3D Slicer as an image computing platform for the Quantitative Imaging Network. Magn Reson Imaging. 2012;30(9):1323-41.

41. -. Community BO. Blender- a 3D modelling and rendering package [Internet]. Stichting Blender Foundation, Amsterdam; 2018. Available from: http://www.blender.org.

42. Xia P, Murray E. 3D treatment planning system-Pinnacle system. Med Dosim. 2018;43(2):118-28.

Appendices

Appendix A

Technical details of the four scanners compared during the Master Thesis project

Table 5 Technical details of the four scanners compared during the Master Thesis project

Specification	Trios Intraoral Scanner	EinScan Einstar	EinScan H2[1]	EinScan SP v2
Technology	Confocal microscopy principles	Structured Light	Structured Light	Structured Light
Scanning Method	Intraoral handheld	Handheld	Handheld	Tabletop scanner
Accuracy	6.9 ± 0.9 µm	Up to 0.1mm	up to 0.05 mm	< 0.05 mm
Scan Speed (single surface no colour)	-	< 1.5 seconds	< 1.5 seconds	< 2 seconds
Scan Volume (Max)	-	200 x 150 x 150 mm	200 x 150 x 150 mm	1200 x 1200 x 1200 mm
Depth of Field	-	300 - 1000 mm	300 - 1000 mm	400 mm
Texture Scanning	Yes	Yes	Yes	Yes
Colour Scanning	Yes	Yes	Yes	Yes
Light Source	-	White Light	White Light	White Light
Connectivity	USB	USB, Wi-Fi	USB, Wi-Fi	USB, Wi-Fi
Software Compatibility	TRIOS Software	EinScan Software	EinScan Software	EinScan Software
Supported File Formats	STL, OBJ, PLY	STL, OBJ, PLY, ASC	STL, OBJ, PLY, ASC	STL, OBJ, PLY, ASC

Appendix B

Schematic drawing of the inlay 3D print design

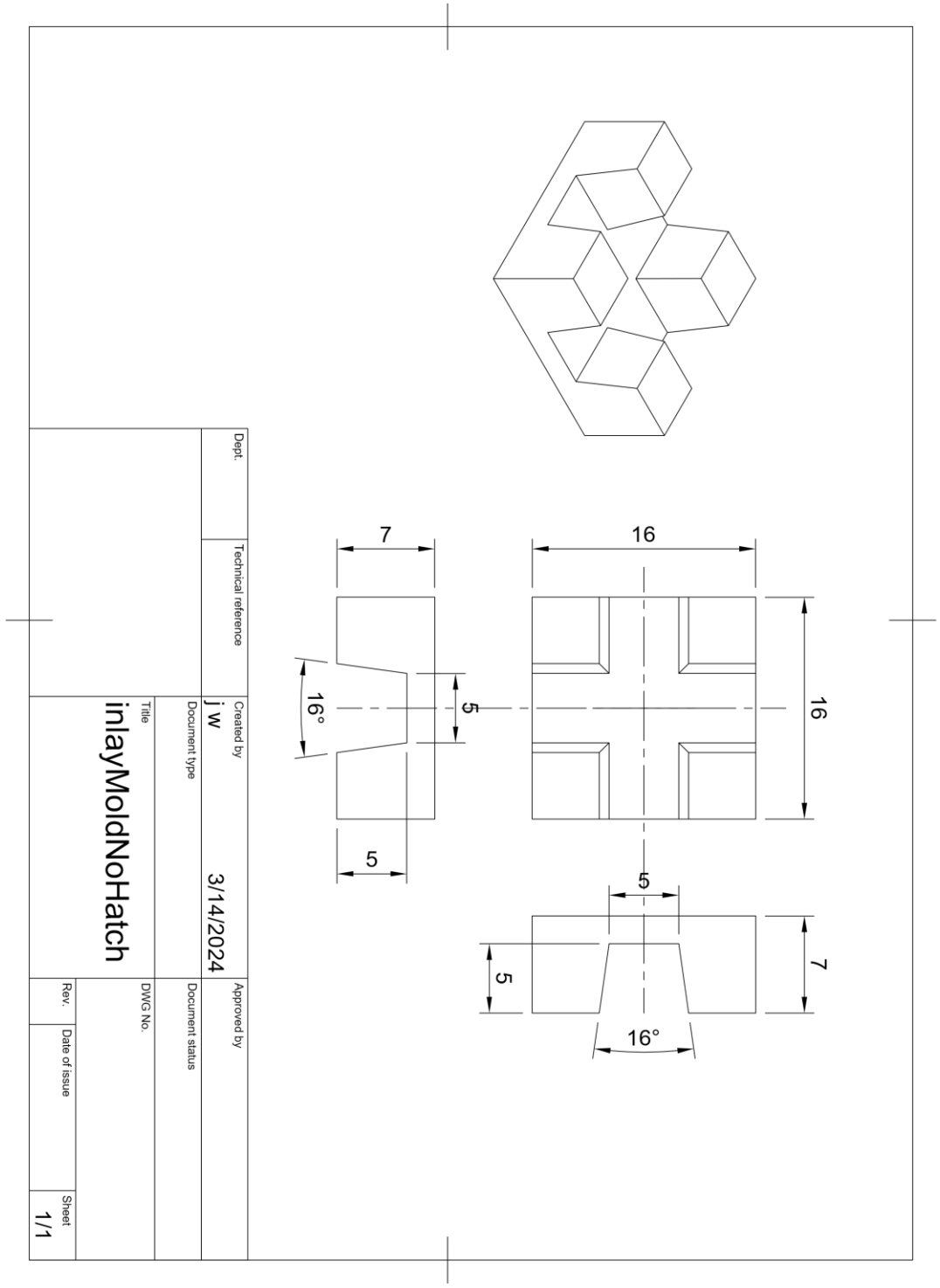

Appendix C

Schematic drawing of the crown and bridge 3D print design

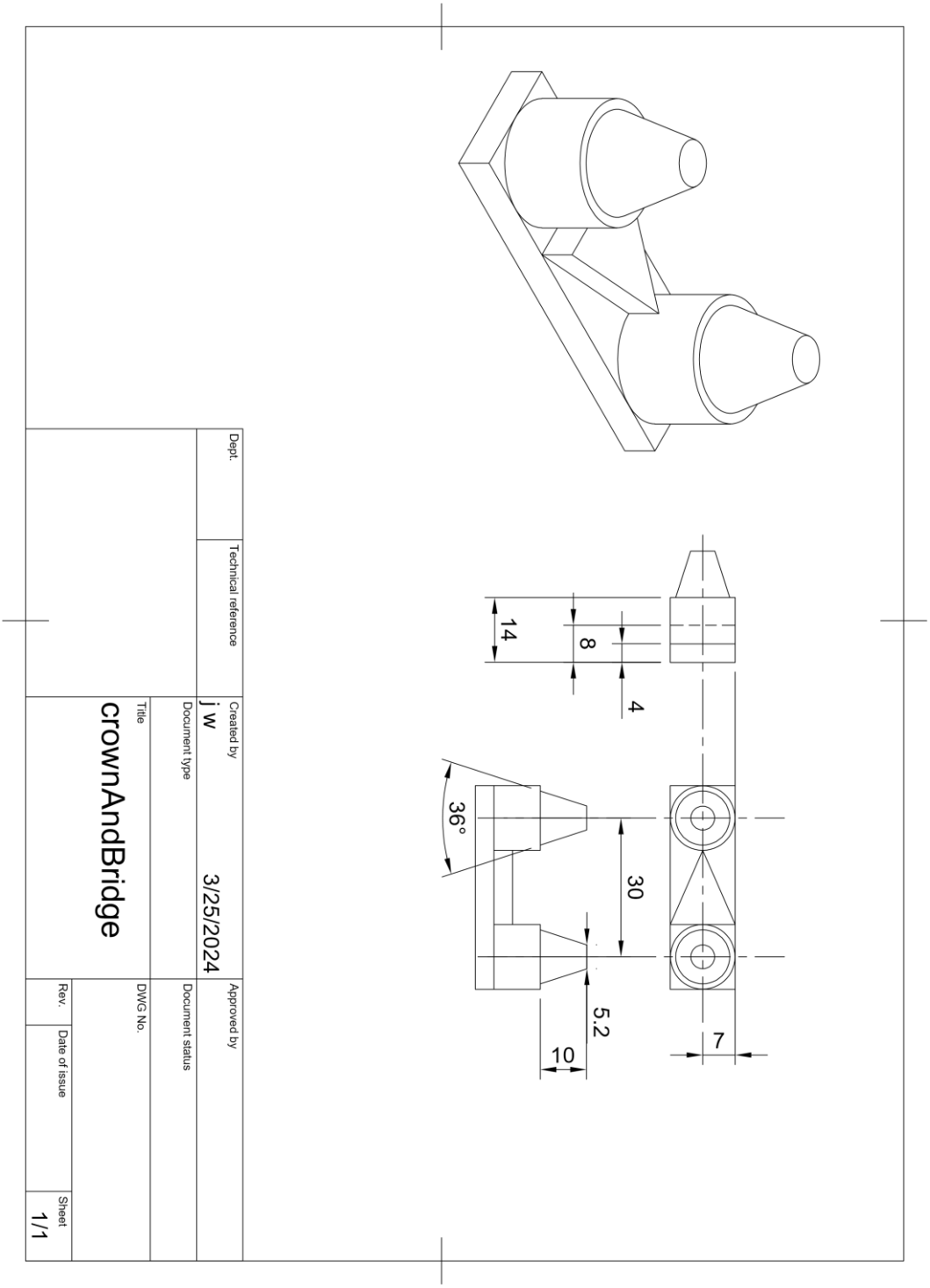

Appendix D

Method of measurements of the 3D printed models

inlay model

measurepoint 1 (sides 16mm)

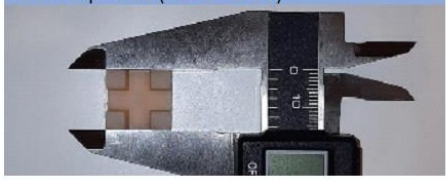

measurepoint 2 (height 7mm)

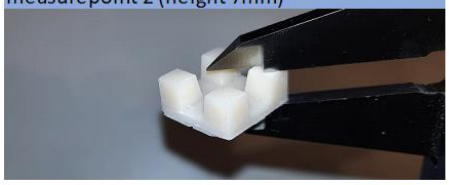

measurepoint 3 (inner cut (5mm)

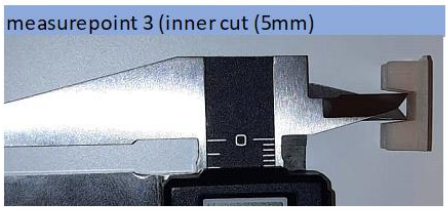

measurepoint 4 (lower plane height)

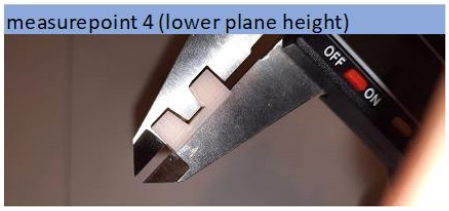

measurepoint 5 (depth 5mm)

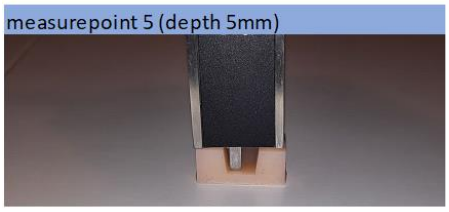

crown and bridge

measurepoint 1 (lower plane 4mm)

measurepoint 2 (middle plane 8mm)

measurepoint 3 (upper middle plane 14mm)

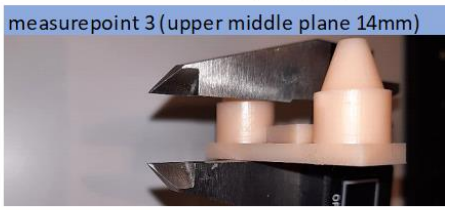

measurepoint 4 (max height 24mm)

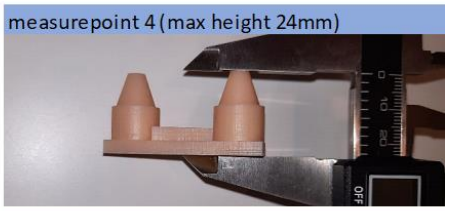

measurepoint 5 (width 14mm)

measurepoint 6 (length 44mm)

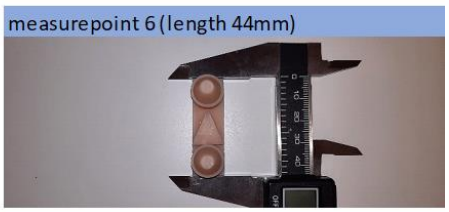

measurepoint 7 (height tower 10mm)

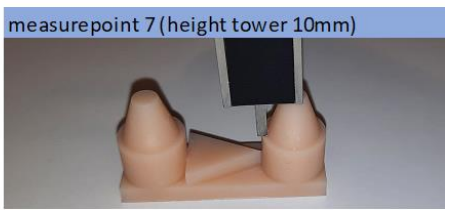

Appendix E

System Usability Scale (SUS)

Rate the following statements from 1 to 5, where:

1 = Strongly Disagree
2 = Disagree
3 = Neutral
4 = Agree
5 = Strongly Agree

Statement	Score
1. I think that I would like to use this scanner frequently.	
2. I found the scanner unnecessarily complex.	
3. I thought the scanner was easy to use.	
4. I think I would need the support of a technical person to be able to use this scanner.	
5. I found the various functions in this scanner were well-integrated. 5	
6. I thought there was too much inconsistency in this scanner.	
7. I would imagine that most people would learn to use this scanner very quickly.	
8. I found the scanner very cumbersome to use.	
9. I felt very confident using the scanner.	
10. I needed to learn a lot of things before I could get going with this scanner.	
SUS Score 2.5 x ((sum of all odd numbered statements – 5) + (25 - sum of all even numbered statements))	

Appendix F

Beknopte Handleiding 3D

Algemeen

De belangrijkste componenten van de 3D-Scanner zijn een camera, een draaiplateau en een combi-statief voor camera en draaiplateau. Verder zijn er naast de netvoedingskabel een micro USB-kabel die de camera met het draaiplateau verbindt en een USB-kabel voor de verbinding met een computer.

Voor het scannen wordt de camera en het draaiplateau op het statief geplaatst en met elkaar verbonden (micro USB-kabel). Verder wordt de camera verbonden met de computer en aangesloten op de netstroom.

Kalibreren

Zet de camera aan (knop licht op) en open vervolgens de EXScan software op de computer.

Als hiertoe aanleiding is geeft het programma aan dat de 3D-Scanner moet worden gekalibreerd (ca. elke 2 weken). Volg hiervoor de Instructies op het scherm.

De beste scanresultaten worden verkregen als er zo weinig mogelijk licht op het te scannen gebied valt. Ook de kalibratie kan het beste onder deze omstandigheden worden uitgevoerd.

Scannen

Leg voordat je een preparaat op het plateau plaatst een vel plasticfolie hierop om dit tegen bloed e.d. te beschermen.

Om de scan te starten kiest je in het EXScan programma ‘New Work’. Daarna moet je een nieuwe map aanmaken om de scan op te slaan. Gebruikt bij voorkeur het format JJJJ-MM-DD_PREPARAATNAAM.

In het venster ‘New Project’ kiest je vervolgens voor ‘Texture Scan’ om een gekleurde scan te maken. Het is niet nodig om ‘Global Markers’ te selecteren.

Nu kunt je de vaste instellingen (menu links in scherm) aanpassen. Voor een standaard scan zet je HRD UIT, Draaiplateau AAN, Align Mode op ‘Turntable Aligned’ en voor de draaiplateau instellingen kies je: Steps 8, Speed 10 en Turns op ‘one turn’.

Tot slot pas je de helderheid aan. Hierbij geeft rood de mate van belichting aan. Zacht weefsel moet nog rood kleuren maar harde objecten (bijv. bot) moeten niet overbelicht worden waardoor detail verloren gaat. Als je een goede afstelling hebt gevonden kan met de spatiebalk de scan worden gestart. Een scan bestaat uit meerdere opnames (een voor elke positie (aantal steps) van het draaiplateau).

Als de scan is voltooid kun je het resultaat beoordelen: liggen alle scangegevens binnen de met groene stippen aangegeven marge en/of zijn er elementen die niet aan de scan zijn gerelateerd (niet verbonden met het model). Met het vinkje aan de rechterzijde van het scherm kan je aangeven dat je het resultaat accepteert en verder gaat met het scannen van de andere zijde van het preparaat.

Draai het preparaat om zodat je de andere zijde kunt scannen. Let op dat je de oriëntatie van het preparaat behoudt (vooral bij weke delen van belang).

Controleer de helderheid en pas deze eventueel aan voordat je met de spatiebalk de tweede scan start.

Uitlijning

Je hebt twee scans (voor- en achterzijde of boven- en onderzijde). Het programma zal proberen deze twee scans automatisch te koppelen zodat één 3D model ontstaat. Lukt dit niet dan kun je de twee delen handmatig samenvoegen.

Selecteer de uitlijnknop (rechterzijde scherm). Sleep nu scan 1 naar het deelscherm 'Fixed' en scan 2 naar het deelscherm 'Floated'. Zorg ervoor dat de oriëntering van de twee scans overeenkomt; als je ze over elkaar heen legt 'passen' ze. Met de linkermuisknop kunt je nu de 'Floated' afbeelding roteren om duidelijke oriëntatiepunten te vinden. Je kunt vervolgens met shift-linkermuisknop gemeenschappelijke punten van de twee helften selecteren. Herhaal dit proces totdat je drie punten hebt geselecteerd (bij voorkeur op verschillende delen van het preparaat).

Opm.: Weke delen van het preparaat zijn minder geschikt om overeenkomende punten te selecteren omdat deze bij het omdraaien van het preparaat vervormt kunnen zijn.

Resultaat vastleggen

Indien de uitlijning goed is klik je linksonder in het scherm op de knop 'Complete' om de 3D-scan vast te leggen. Vervolgens kan je 'Global Optimalization' kiezen waarmee de 'meshing' slecht uitgelijnde gebieden corrigeert. Je doorloopt nu verschillende optimalisatieschermen die steeds met een vinkje (bevestiging) worden afgesloten. Als het optimalisatieproces is voltooit kies je rechtsonder op het scherm 'Mesh Model', 'Watertight Model'.

Je kan kiezen voor verschillende gradaties van detaillering. Hoe hoger de mate van detail hoe langer de computer moet rekenen. Als je een snel resultaat nodig hebt, kies dan voor 'Low Detail'. In de andere gevallen voldoet 'Medium Detail' (High Detail is visueel niet significant beter maar het renderen duurt veel langer).

Nadat je de helderheid en het contrast hebt gekozen kunt je met 'Save Your Scan' uw Scan opslaan. Om de afmetingen van het preparaat te behouden hou je de schaal op 100%.

Het resultaat kan je opslaan in de map die je aan het begin van de scan hebt aangemaakt. Gebruik de eerder aangegeven conventie voor de naam en kies voor het bestandtype .stl, .ply, .3MF en/of .OBJ. Deze bestandtypen zijn onderaan het venster weergegeven en aan te vinken.

Appendix G

DATA REMOVED FOR PRIVACY REASONS

END OF DOCUMENT